Journal of Theoretical and Applied Mechanics, Sofia, Vol.52 (2022) pp. 179-196
FLUID MECHANICS

BOUNDARY LAYER FLOW OF A CONDUCTING HYPERBOLIC NANOFLUID OVER A STRETCHING SURFACE WITH CHEMICAL REACTION AND HEAT SOURCE/SINK

S. VENKATESWARLU[1], S.V.K. VARMA[2],
R.V.M.S.S KIRAN KUMAR[3*]

[1]*Department of Mathematics, Vikrama Simhapuri University College, Kavali-524201, A.P, India*
[2]*Department of Mathematics, School of Applied Sciences, REVA University, Bengaluru-560064, Karnataka, India*
[3]*Government Polytechnic College, Anantapur-515002, A.P, India*

[Received: 08 May 2021. Accepted: 05 April 2022
doi: https://doi.org/10.55787/jtams.22.52.2.179

ABSTRACT: In this article, a steady incompressible stagnation point flow of a conductive hyperbolic radiative nano-liquid past a stretching surface is investigated. The effects of heat generation/absorption and first-order destructive chemical reactions are considered. The Buongiorno's nanofluid model is used to study the combined effects of thermophoresis and Brownian motion. The governing higher order non-linear partial differential equations (PDE's) are transformed to a set of ordinary differential equations (ODE's) by applying suitable similarity relations. The resulting ordinary differential equations are numerically solved with the help of a boundary value problem default solver in MATLAB bvp4c tool. The attitude of fluid velocity, temperature and concentration on various flow quantities are analyzed through tables and figures. From the outcomes, we observed that for raising the values of Weissenberg's number the fluid velocity is diminished.

KEY WORDS: hyperbolic nanofluid, Hartmann number, radiative heat flux, heat source, chemical reaction.

NOMENCLATURE

(u, v)	Velocity components in $(x,\ y)$ directions	u_e	Free stream velocity
B_0	Magnetic field strength	T	Dimensional temperature
C	Dimensional concentration	C_p	Heat capacity at constant pressure
ν	Kinematic viscosity	ρ	Fluid density
R	Radiation parameter	n	Power law index
τ	Ratio of specific heats	D_B	Coefficient of Brownian motion

*Corresponding author e-mail: rsai.maths@gmail.com

D_T	Coefficient of thermophoresis diffusion	k_l	Chemical reaction coefficient
k	Thermal conductivity	Pr	Prandtl number
M	Hartmann's number	A	Stretching ratio parameter
Nb	Dimensionless Brownian motion parameter	Nt	Dimensionless thermophoresis parameter
Cf	Friction factor coefficient	We	Weissenberg's number
Nu_x	Rate of local heat transfer coefficient	Sh_x	Rate of local mass transfer coefficient
Q_0	Dimensional Heat generation/ absorption coefficient	Q	Heat generation/ absorption parameter
Sc	Schmidt number	S	Suction/injection parameter
Kr	Destructive/generative chemical reaction parameter	q_w	Heat flux
		q_m	Mass flux
Re_x	Reynolds number	f	Dimensionless velocity
a, c	Constants		

Greek Symbols

η	Similarity variable	σ	Electrical conductivity
Γ	Time constant (or material constant)	α	Thermal diffusivity
θ	Dimensionless temperature	ϕ	Dimensionless concentration
μ	Dynamic viscosity	τ_w	Sheet shear stress

Subscripts

∞	Ambient condition	w	Condition on the sheet or wall

Superscripts

$'$	Differentiation w.r.t η	$*$	Dimensional properties

1 INTRODUCTION

The study of boundary layer behavior induced by a stretching surface is attractive to the modern investigators due to its wide range of applications in engineering processes, for example, freezing of an infinite metallic plate in paper production, condensation on the process, tinning of copper wire, etc. It is noticed that extensive studies on this topic have been taking on for a linearly stretching surface. Sakiadis [1] expressed the steady 2D flow pattern over solid surfaces moving with constant speed. Stretched flow caused by a surface was investigated by Crane [2]. The heat transfer characteristics over a continuous stretching surface were examined by Ali [3]. Cortell [4] studied the stretched flow by considering radiation. Later, Srinivas et al. [5] examined the influence of fluid temperature and concentration over a stretching surface.

Many of the investigations on Newtonian fluids over a stretching surface were done by several authors. But in spite of many real-life applications of non-Newtonian fluids, the investigators focused on non-Newtonian fluids, and they found different types of non-Newtonians rheological models. Among them, the tangent hyperbolic liquid model is one of the basic models which essentially depict the shear-diminishing

properties of the liquid. The peristaltic stream model of an exaggerated digression liquid in a vertical asymmetric channel in the conducting field was presented by Nadeem and Akram [6]. Afterwards, Nadeem and Maraj [7] broke-down the peristaltic stream of hyperbolic tangent fluid in a bended channel. Akbar et al. [8] have examined the hyperbolic liquid flow over an extending surface in a conducting field. Later, Kumar et al. [9] investigated the peristaltic transport of hypergolic liquid through a slanted channel. Abdul et al. [10] discussed the flow of a hyperbolic liquid from a sphere with convective conditions. They found that the liquid velocity and temperature are the expanding elements of the Biot number. The hydromagnetic boundary layer stream of a hyperbolic liquid over a stretching cylinder is investigated by Malik et al. [11]. Reddy et al. [12] examined the heat and mass transfer effects on hyperbolic liquid under the conducting field; they presumed that the velocity diminishes with the power-law parameter. Further, various hypothetical and trial examinations on hyperbolic liquid were finished by various scientists [13–18].

In 1995, Choi and Eastman [19] found another sort of conventional liquid to beat the thermal conductivity of ordinary liquids. Consequently, in the accompanying examinations, the investigators contemplated the stream investigation by considering the hyperbolic nano-liquid. Hayat et al. [20] introduced the peristaltic movement of hyperbolic nanofluid in a conducting slip flow by considering Joule heating. They noticed the contrary behavior of thermophoresis and Brownian motion effects on species diffusion. The hydrodynamic progression of a hyperbolic liquid with nanoparticles over a stretching sheet was concentrated by Ibrahim [21]. He observed that the Weissenberg's number and power-law parameters expand the obstruction of the flow, which diminishes the stream field. The flow of a hydrodynamic hyperbolic nano-liquid stream was numerically examined by Khan et al. [22]. The flow of a hyperbolic nanofluid over a variable thickness surface was concentrated by Hayat et al. [23]. The magnetohydrodynamic delineated flow of a hyperbolic nanofluid over a slanted plate was explored by Hayat et al. [24]. Also, the heat and mass transfer significances for hyperbolic nanofluid are concentrated by Shahzad et al. [25]. The authors [25] have noted the contrary pattern for destructive and constructive reactions. Further, they observed the enhancement of thermal boundary layer thickness with increasing values of Brownian motion and thermophoresis parameters. The impact of copper nanoparticles on hydromagnetic hyperbolic liquid over a fallopian tube was analyzed by Maqbool et al. [26]. The hydromagnetic boundary layer unsteady flow of a hyperbolic nanofluid over a moving stretching cylinder was examined by Gharami et al. [27]. They concluded that the hyperbolic liquid impacted the properties of heat and mass transfer significantly instead of conventional liquids.

Enlivened by the above examinations, the main objective of this investigation is to analyze the heat and mass transfer impacts on a 2D stagnation point flow of a

tangent hyperbolic liquid over a stretching surface. The modeled non-linear ODE's are comprehended with MATLAB bvp4c package. The impact of interesting physical quantities is computed and explained through figures and tables. Moreover, we compared the results of the present method with the current outcomes.

2 Formulation of the Model

A steady 2D flow of a viscous incompressible hyperbolic nano-liquid over a stretching sheet is considered. The sheet is stretched along the$X-$direction (flow direction). The sheet velocity and ambient velocity is considered as $u_w(x) = cx$ and $u = u_e(x) = ax$ respectively. A magnetic field of strength B_0 is applied opposite to the surface, which is appeared in Fig. 1. Furthermore, the Reynolds number is thought to be minuscule, accordingly, the induced magnetic field is ignored. Additionally, electric field impact, viscous dissipation impact, and Joule heating are disregarded. The radiative heat flux is described by using the Rosseland approximation in the energy equation and it is applied along the $X-$direction. The numerical conditions are developed by consolidating the non-homogenous nanofluid model and tangent hyperbolic model.

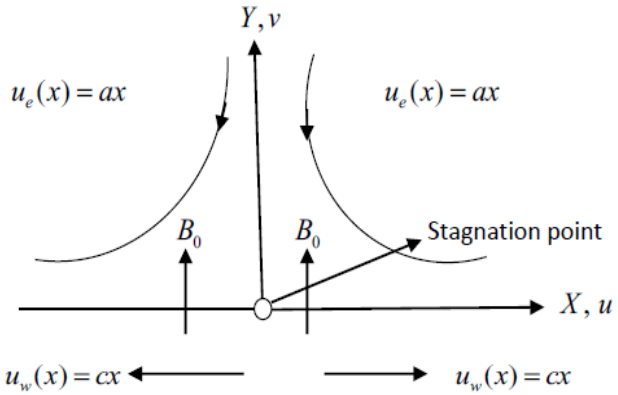

Fig. 1: Schematic representation of the flow.

Under the above boundary layer presumptions, the governing boundary layer equations of a tangent hyperbolic nanofluid model are given below [8, 28].

$$\frac{\partial u}{\partial x} + \frac{\partial v}{\partial y} = 0, \tag{1}$$

$$u\frac{\partial u}{\partial x} + v\frac{\partial u}{\partial y} = \nu(1-n)\frac{\partial^2 u}{\partial y^2} + \sqrt{2}\nu n\Gamma\left(\frac{\partial u}{\partial y}\right)\left(\frac{\partial^2 u}{\partial y^2}\right) + u_e\frac{du_e}{dx} - \frac{\sigma B_0^2 u}{\rho}, \tag{2}$$

$$u\frac{\partial T}{\partial x}+v\frac{\partial T}{\partial y}=\alpha\frac{\partial^2 T}{\partial y^2}+\tau\Big[D_B\Big(\frac{\partial C}{\partial y}\Big)\Big(\frac{\partial T}{\partial y}\Big)+\frac{D_T}{T_\infty}\Big(\frac{\partial T}{\partial y}\Big)^2\Big] - \frac{16\sigma^* T_\infty^3}{3(\rho C_p)k^*}\frac{\partial^2 T}{\partial y^2}+\frac{Q_0}{\rho C_p}(T-T_\infty), \tag{3}$$

$$u\frac{\partial C}{\partial x}+v\frac{\partial C}{\partial y}=D_B\frac{\partial^2 C}{\partial y^2}+\frac{D_T}{T_\infty}\Big(\frac{\partial^2 T}{\partial y^2}\Big)-k_l(C-C_\infty). \tag{4}$$

Relating boundary layer conditions are

$$\begin{aligned} &u=u_w(x)=cx, \quad v=v_w, \quad T=T_w, \quad C=C_w \quad \text{at } y=0,\\ &u\to u_e(x)=ax, \quad T\to T_\infty, \quad C\to C_\infty \quad \text{as } y\to\infty\,. \end{aligned} \tag{5}$$

The dimensional partial differential conditions (2) – (4) and the boundary conditions (5) are changed into dimensionless structure by utilizing the accompanying relations

$$\begin{aligned} &\eta=y\sqrt{\frac{c}{\nu}}, \quad u=cxf'(\eta)\,, \quad v=-\sqrt{c\nu}f(\eta),\\ &\theta(\eta)=\frac{T-T_\infty}{T_w-T_\infty}\,, \quad \phi(\eta)=\frac{C-C_\infty}{C_w-C_\infty}\,. \end{aligned} \tag{6}$$

Taking into account the above changes, the governing partial differential equations (PDE's) becomes:

$$(1-n)f'''+nWef'''f''+ff'-f'^2+A^2-Mf'=0\,, \tag{7}$$

$$f\theta'+\frac{1}{\Pr}\theta''+Nb\theta'\phi'+Nt\theta'^2+\frac{4}{3\Pr}R\theta''+Q\theta=0\,, \tag{8}$$

$$f\phi'+\frac{1}{Sc}\phi''+\frac{1}{Sc}\Big(\frac{Nt}{Nb}\Big)\theta''-Kr\phi=0 \tag{9}$$

and the boundary layer approximations are:

$$\begin{aligned} &f=S, \quad f'=1, \quad \theta=1, \quad \phi=1 \quad \text{at } \eta=0,\\ &f'\to A, \quad \theta\to 0, \quad \phi\to 0 \quad \text{as } \eta\to\infty\,. \end{aligned} \tag{10}$$

In the dimensionless ordinary equations

$$M=\frac{\sigma B_0^2}{\rho c}\,, \quad We=\sqrt{\frac{2}{\nu}}c^{\frac{3}{2}}x\Gamma\,, \quad \Pr=\frac{\nu}{\alpha}\,, \quad Sc=\frac{\nu}{D_B}\,,$$
$$Nt=\frac{\tau D_T(T_w-T_\infty)}{\nu}\,, \quad Nb=\frac{\tau D_B(C_w-C_\infty)}{\nu}\,, \quad S=-\frac{v_w}{\sqrt{c\nu}}\,, \quad A=\frac{a}{c}\,,$$
$$Q=\frac{Q_0}{c(\rho C_p)}\,, \quad R=\frac{4\sigma^* T_\infty^3}{kk^*}\,, \quad Kr=\frac{k_l}{c}\,.$$

2.1 PHYSICAL QUANTITIES

The friction at the surface, local heat transfer rate and local mass transfer rate are defined as

$$Cf = \frac{\tau_w}{\frac{1}{2}\rho u_w^2}, \quad Nu_x = \frac{xq_w}{k(T_w - T_\infty)}, \quad Sh_x = \frac{xq_m}{D_B(C_w - C_\infty)}, \tag{11}$$

where

$$\begin{aligned} \tau_w &= (1-n)\Big(\frac{\partial u}{\partial y}\Big)_{aty=0} + \frac{n\Gamma}{\sqrt{2}}\Big(\frac{\partial u}{\partial y}\Big)^2_{aty=0}, \\ q_w &= -k\Big(\frac{\partial T}{\partial y}\Big)_{aty=0}, \quad q_m = -D_B\Big(\frac{\partial C}{\partial y}\Big)_{aty=0}. \end{aligned} \tag{12}$$

Considering conditions (12), we obtained

$$\begin{aligned} \frac{CfRe_x^{\frac{1}{2}}}{2} &= (1-n)f''(0) - \frac{nWe}{2}f'''^3(0), \\ Nu_x Re_x^{-\frac{1}{2}} &= -\theta'(0), \\ Sh_x Re_x^{-\frac{1}{2}} &= -\phi'(0), \end{aligned} \tag{13}$$

where the local Reynolds number is defined as $Re_x = \dfrac{u_w x}{\nu}$.

3 NUMERICAL SOLUTION

The group of non-linear dimensionless equations (7) – (9) with the related conditions (10) is simplified by utilizing bvp4c, which incorporates Runge-Kutta (RK) fourth-order shooting technique, which is typically a collocation of fourth order. Here, the error mechanism and mesh choice are set up by the remaining of the continuous solution. In this mechanism, the choice of $\eta_\infty = 5$, ensures that each solution approach asymptotic values precisely.

4 NUMERICAL RESULTS AND DISCUSSION

The acquired outcomes are examined and analyzed through Figs. 2–15 and Table 1. Additionally, the current outcomes are affirmed with the existing results of Akbar et al. [29], Malik et al. [30], and Khan et al. [31] (see Table 2). All through our investigation we fixed the accompanying qualities for mathematical computation as $n = 0.5$, $We = 0.3$, $M = 0.5$, $Pr = 6.8$, $R = 0.2$, $Nb = 0.2$, $Nt = 0.3$, $Q = 0.5$, $Sc = 0.1$, $Kr = 0.5$, $S = 0.6$, $A = 0.5$.

Table 1: Variations in Cf, Nu_x and Sh_x versus flow parameters

n	M	We	Nb	Nt	Q	Kr	Cf	Nu_x	Sh_x
0.1							1.069162	0.478973	0.051099
0.2							1.175806	0.468636	0.065362
0.3							1.325554	0.456465	0.082214
	0.1						1.660384	0.477180	0.054982
	0.3						1.801680	0.458776	0.079965
	0.5						2.108973	0.421756	0.130569
		0.1					1.701013	0.432055	0.116132
		0.2					1.871487	0.427514	0.122494
		0.3					2.209319	0.421756	0.130569
			0.5				2.209357	0.355260	0.318634
			1				2.209357	0.250238	0.379569
			1.5				2.209357	0.153356	0.398252
				0.1			2.209319	0.462033	0.276870
				0.2			2.209319	0.441819	0.194013
				0.3			2.209319	0.421756	0.130569
					0.2		2.209293	0.663395	-0.223125
					0.4		2.209293	0.511520	-0.000719
					0.6		2.209293	0.318825	0.280981
						1	2.209319	0.418120	0.214174
						2	2.209319	0.418120	0.358748
						3	2.209319	0.418120	0.480845

Table 2: Comparison results of Hartmann number (M) with the existing outcomes

M	Akbar et al. [29]	Malik et al. [30]	Khan et.al. [31]	Present results
0	-1	-1	-1	-1
0.5	-1.118803	-1.11802	-1.1180	-1.1181
1.0	-1.41421	-1.41419	-1.4139	-1.4135
5	-2.449449	-2.44945	-2.4499	-2.4498
10	-3.31663	-3.31657	-3.3170	-3.3168
100	-10.0498	-10.0498	-10.0503	-10.0501
500	-22.38303	-22.38294	-22.3839	-22.3827
1000	-31.63859	-31.63851	-31.6399	-31.6372

The impact of Hartmann's number (M) on fluid velocity, temperature, and concentration fields are appeared in Figs. 2–3. From Fig. 2, it is seen that the enhancement of Hartmann number causes decreases in velocity profiles. This is due to the

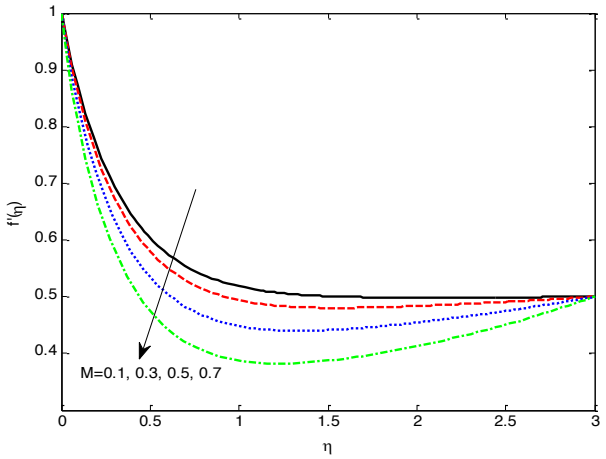

Fig. 2: Effect of M on $f'(\eta)$.

fact that the enormous values of the Hartmann number produce Lorentz force, which restricts the movement of the stream, yet the contrary phenomenon is seen in Fig. 3. Moreover, the reduction in energy boundary layer thickness is noticed. Fig. 4 reveals the behavior of Weissenberg number (We) and it decelerates the velocity of the fluid. Since Weissenberg number is proportional to relaxation time, consequently, its bigger values upgrade the relaxation time, so it offers more obstruction in a liquid movement that naturally diminishes liquid velocity. The influence of the stretching ratio parameter on velocity is shown in Fig. 5. It is seen that when the free stream velocity is bigger

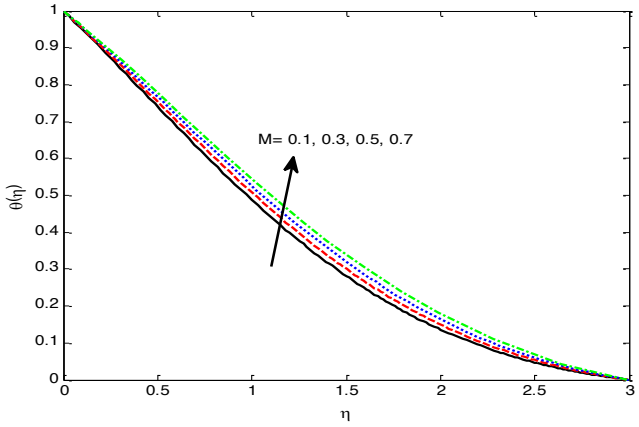

Fig. 3: Effect of M on $\theta(\eta)$.

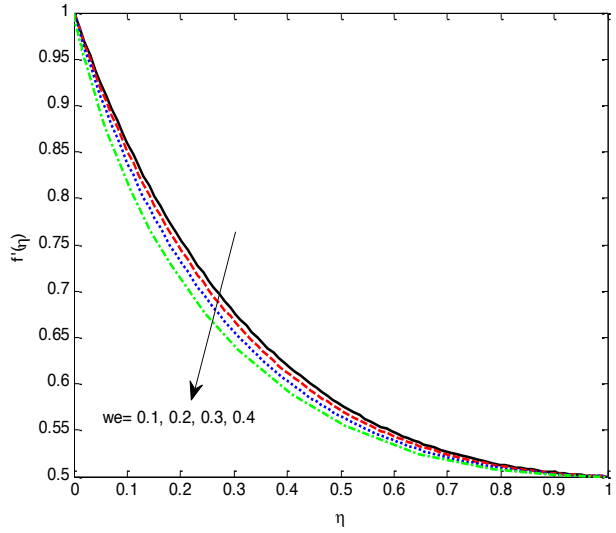

Fig. 4: Effect of We on $f'(\eta)$.

than the stretching velocity of the sheet, the liquid velocity raises and the boundary layer thickness reduces with upgrading stretching ratio parameter (A). Besides, the nano-liquid velocity diminishes and boundary layer thickness rises monotonically, if free stream velocity is smaller than the stretching velocity of the sheet. The liquid

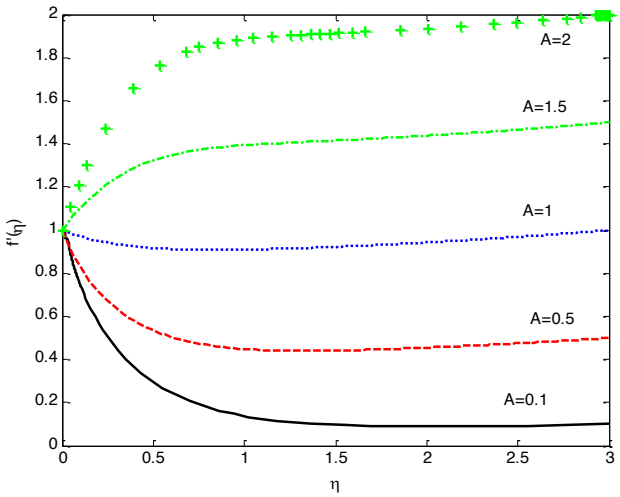

Fig. 5: Effect of A on $f'(\eta)$.

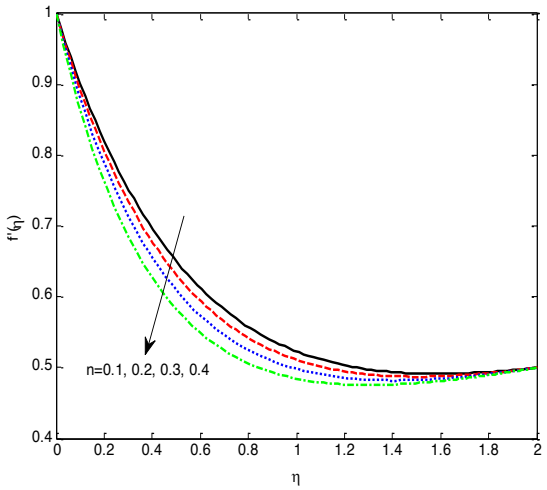

Fig. 6: Effect of n on $f'(\eta)$.

velocity diminishes for bigger estimations of the power-law index parameter (n) (see Fig. 6). The liquid changes its tendency from shear-thinning to shear thickening when n increases. Thus, we can see various types of liquids dependent on the estimations of n. Figure 7 shows the impact of suction on the fluid velocity in two different cases of velocity ratio parameter, and seen that with an expansion in the magnitude of suction parameter (S), the velocity appropriation is found to decrease. This is a result

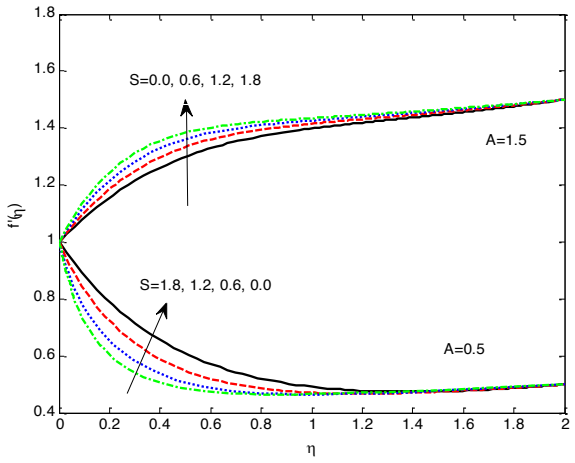

Fig. 7: Effect of S on $f'(\eta)$.

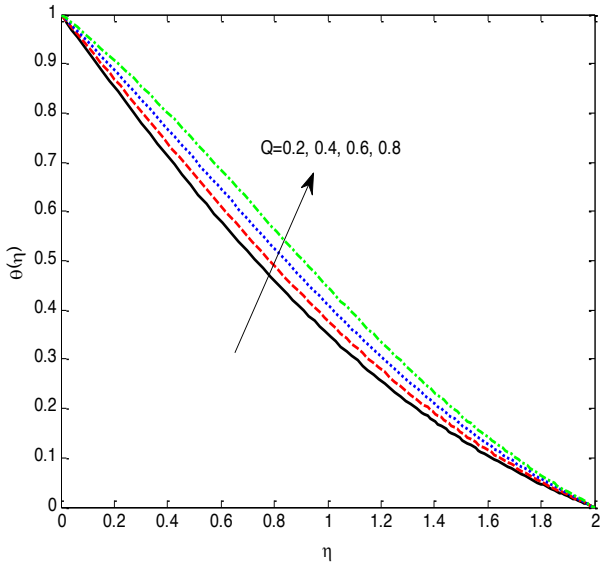

Fig. 8: Effect of Q on $\theta\,(\eta)$.

of the fact that the suction/injection prompts liquid velocity decline/increment hydromagnetic boundary layer. Likewise, from the figure, we conclude that the suction parameter is inversely proportional to the velocity ratio parameter.

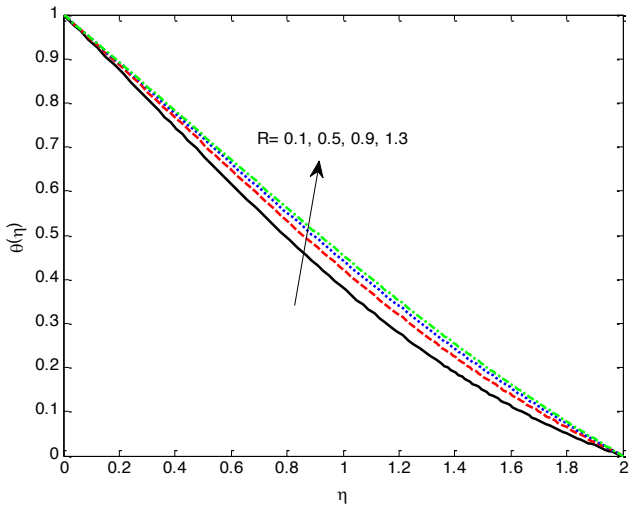

Fig. 9: Effect of R on $\theta\,(\eta)$.

Figure 8 displays the fluid temperature outline for the diverse values of the non-uniform heat absorption/generation parameter (Q). It is expressed that the boundary layer creates the energy, which causes the temperature report to upgrade with raising estimations of heat source $(Q > 0)$, though for the situation of absorption $(Q < 0)$ reverse phenomena is observed. Figure 9 illustrates the impact of the radiation parameter (R) on the nanoparticle temperature field. The radiation factor is responsible for the thickening of the energy boundary. This empowers the liquid to release the heat from the flow region and makes the system cool. This is due to the fact that the Rosseland approximation results improve in temperature. The impact of Brownian motion on fluid temperature is shown in Fig. 10. It is seen from the figure that, as the estimations of the Brownian motion factor (Nb) increases the random movement of fluid particles, which accelerates the fluctuations among them, subsequently raises the temperature of the liquid and the boundary layer width. But the opposite pattern is seen on the concentration field (see Fig. 11). Truly, a raise in Brownian motion causes inconsistent development of nanoparticles, subsequently, depreciates the nanoparticle concentration and boundary layer thickness.

The impact of the thermophoresis factor (Nt) on temperature is inspected from Fig. 12. The higher values of thermophoresis parameter raise the liquid particles transfer from hot state to cold state, thus the liquid temperature and the boundary layer thickness raises. A similar conduct is seen in concentration with expanding thermophoresis parameter (see Fig. 13). Figure 14 shows the conduct of Schmidt

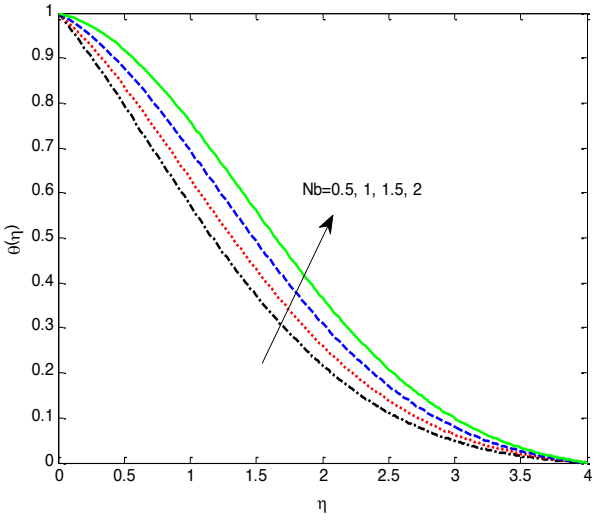

Fig. 10: Effect of Nb on $\theta\,(\eta)$.

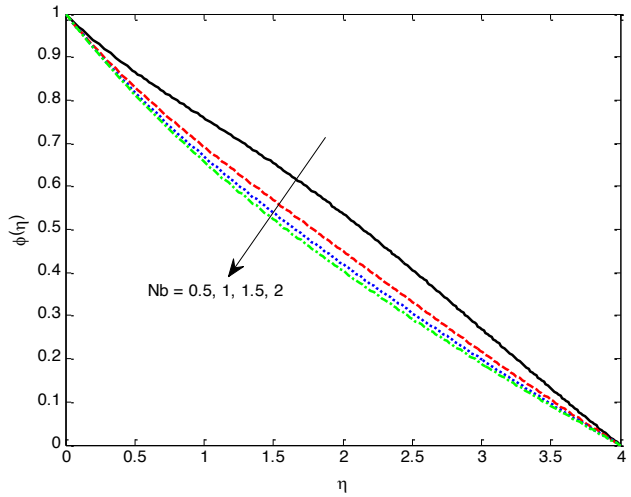

Fig. 11: Effect of Nb on $\phi\,(\eta)$.

number (Sc) on the concentration field. It is seen that by expanding the Schmidt number the concentration profile diminishes. Since Schmidt number is inversely proportional to the molecular diffusivity and thus the concentration profile diminishes. Figure 15 investigates the impact of destructive chemical reaction $(Kr > 0)$ on the concentration filed. In general, the fluid concentration is a diminishing function of

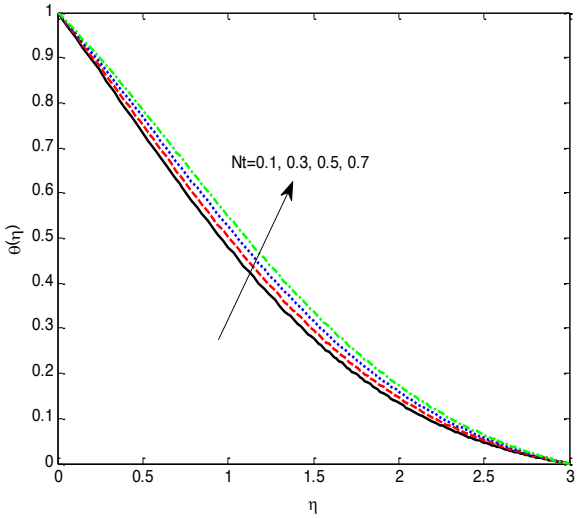

Fig. 12: Effect of Nt on $\theta\,(\eta)$.

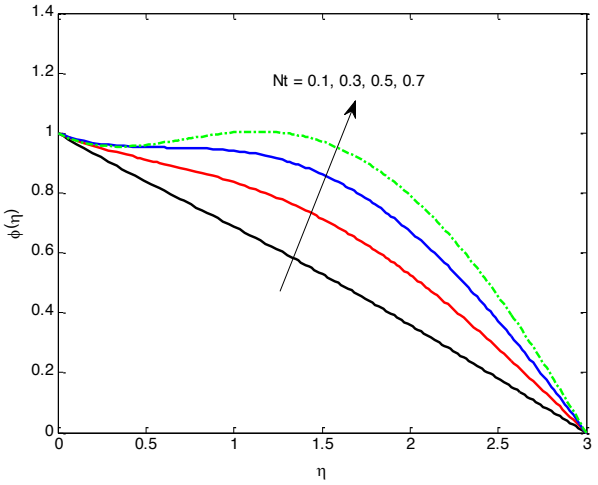

Fig. 13: Effect of Nt on $\phi(\eta)$.

Kr. Since the heat generation is expanded for the bigger estimations of Kr and thus ruins the liquid concentration.

The numerical estimations of the friction factor coefficient and the rate of local heat and mass transfer coefficients for different significant stream quantities are presented in Table 1. It is seen that the friction at the wall increases with an expansion in n, We and M. The rate of heat transfer coefficient diminishes with expanding estimations of n, M We, Nb, Nt, Q and Kr. Besides, the expanding estimations

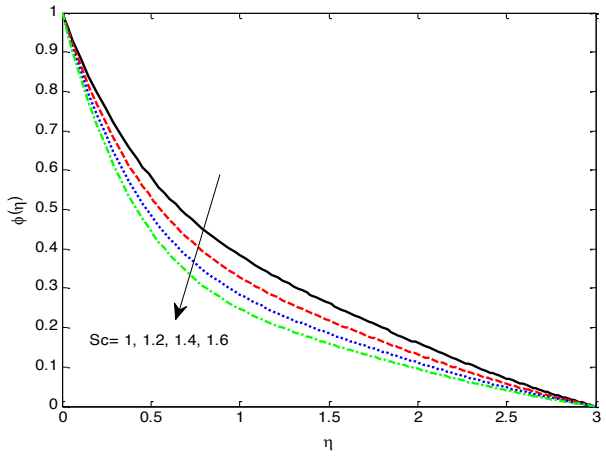

Fig. 14: Effect of Sc on $\phi(\eta)$.

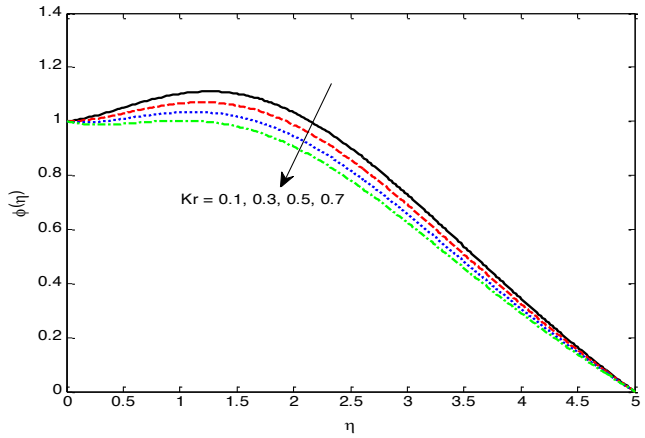

Fig. 15: Effect of Kr on $\phi(\eta)$.

of n, S, We, Nb and Q improves the mass transfer rate, while devalued with Nt. Additionally, no impact of Nb, Nt, Q and Kr on Cf and Kr on Nu_x is noticed.

5 Final Conclusions

The Present examination portrays the mathematical investigation of tangent hyperbolic nano-liquid flow past a stretching sheet within the sight of a magnetic field. The flow pattern is developed by using tangent hyperbolic rheological model. Here the non-comparable results of modeled boundary value problem have been presented and analysed through graphs and tables. The significant results of this problem are given below:

1. The nano-liquid velocity diminishes with the increasing values of magnetic-field parameter, Weissenberg number and power-law index parameter.

2. The Fluid temperature increases for higher values of Brownian motion, thermophoresis, heat source and thermal radiation parameters.

3. The rising values of thermophoresis and Brownian motion parameters reduces the fluid concentration.

4. The species concentration is a decreasing function of the first order chemical reaction parameter.

5. The friction at the wall is an expanding function of magneticfield parameter, Weissenberg number and power-law index parameter.

6. The Heat transfer rate is depreciated for the higher values of Brownian motion and thermophoresis parameters.

7. It is revealed that the local mass transfer rate is an expanding function of chemical reaction parameter, whereas the opposite trend is observed in the case of Brownian motion parameter.

REFERENCES

[1] B.C. SAKIADIS (1961) Boundary layer behavior on continuous solid surfaces: Boundary layer equations for two-dimensional and axisymmetric flow. *Journal of American Institute of Chemical Engineers* (AIChE) **7** 26-28.

[2] L.J. CRANE (1970) Flow past a stretching plate. *Journal of Applied Mathematics and Physics (ZAMP)* **21** 645-647.

[3] M.E. ALI (1994) Heat transfer characteristics of a continuous stretching surface. *Heat and Mass Transfer* **29** 227-234.

[4] R. CORTELL (2013) Fluid flow and radiative nonlinear heat transfer over a stretching sheet. *Journal of King Saud University – Science* **26** 161-167.

[5] S. SRINIVAS, P.B.A. REDDY, B.S.R.V. PRASAD (2014) Effects of chemical reaction and thermal radiation on MHD flow over an inclined permeable stretching surface with non-uniform heat source/sink: an application to the dynamics of blood flow. *Journal of Mechanics in Medicine and Biology* **14** 1-24.

[6] S. NADEEM, S. AKRAM (2011) Magneto hydrodynamic peristaltic flow of a hyperbolic tangent fluid in a vertical asymmetric channel with heat transfer. *Acta Mechanica Sinica* **27** 237-250.

[7] S. NADEEM, E.N. MARAJ (2013) The mathematical analysis for peristaltic flow of hyperbolic tangent fluid in a curved channel. *Communications in Theoretical Physics* **59** 729-736.

[8] N.S. AKBAR, S NADEEM, R.U. HAQ, Z.H. KHAN (2013). Numerical solutions of magneto hydrodynamic boundary layer flow of tangent hyperbolic fluid flow towards a stretching sheet with magnetic field. *Indian Journal of Physics* **87** 1121-1124.

[9] Y.V.K.R KUMAR, P. VINOD KUMAR, S. BATHUL (2014). Effect of slip on peristaltic pumping of a hyperbolic tangent fluid in an inclined asymmetric channel. *Advances in Applied Science Research* **5** 91-108.

[10] S.A. GAFFAR, V.R. PRASAD, O.A. BEG (2015) Numerical study of flow and heat transfer of non-Newtonian Tangent Hyperbolic fluid from a sphere with Biot number effects. *Alexandria Engineering Journal* **54** 829-841.

[11] M.Y. MALIK, T. SALAHUDDIN, H. ARIF, S. BILAL (2015) MHD flow of tangent hyperbolic fluid over a stretching cylinder: Using Keller box method. *Journal of Magnetism and Magnetic Materials* **395** 271-276.

[12] M.G. REDDY, J. MANJULA, P. PADMA (2017) Mass transfer flow of MHD radiative tangent hyperbolic fluid over a cylinder: A numerical study. *International Journal of Applied and Computational Mathematics* **3** 447-472.

[13] K.G. KUMAR, B.J. GIREESHA, N.G. RUDRASWAMY, R.S.R GORLA (2017). Melting heat transfer of hyperbolic tangent fluid over a stretching sheet with fluid particle suspension and thermal radiation. *Communications in Numerical Analysis* **2** 125-140.

[14] M. NASEER, M.Y. MALIK, S. NADEEM, A. REHMAN (2014) The boundary layer flow of hyperbolic tangent fluid over a vertical exponentially stretching cylinder. *Alexandria Engineering Journal* **53** 747-750.

[15] T. HAYAT, S. QAYYUM, B. AHMAD, M., WAQAS (2016). Radiative flow of a tangent hyperbolic fluid with convective conditions and chemical reaction. *The European Physical Journal Plus* **131** 1-13.

[16] A. ALI, R. HUSSAIN, M. MAROOF (2019) Inclined hydromagnetic impact on tangent hyperbolic fluid flow over a vertical stretched sheet. *AIP Advances* **9** 125022.

[17] K.U. REHMAN, A.A. MALIK, M.Y MALIK, N.U. SABA (2017) Mutual effects of thermal radiation and thermal stratification on tangent hyperbolic fluid flow yields by both cylindrical and flat surfaces. *Case Studies in Thermal Engineering* **10** 244-254.

[18] K.G. KUMAR, B.J. GIREESHA, M.R. KRISHNAMURTHY, N.G. RUDRASWAMY (2017) An unsteady squeezed flow of a tangent hyperbolic fluid over a sensor surface in the presence of variable thermal conductivity. *Results in Physics* **7** 3031-3036.

[19] S.U.S. CHOI, J.A. EASTMAN (1995) Enhancing Thermal Conductivity of Fluids with Nanoparticles. *ASME International Mechanical Engineering Congress & Exposition* 1-8.

[20] T. HAYAT, M. SHAFIQUE, A. TANVEER, A. ALSAEDI (2016) Magnetohydrodynamic effects on peristaltic flow of hyperbolic tangent nanofluid with slip conditions and Joule heating in an inclined channel. *International Journal of Heat and Mass Transfer* **102** 54-63.

[21] W. IBRAHIM (2017) Magnetohydrodynamics (MHD) flow of a tangent hyperbolic fluid with nanoparticles past a stretching sheet with second order slip and convective boundary condition. *Results in Physics* **7** 3723-3731.

[22] M. KHAN, A. HUSSAIN, M.Y. MALIK, T. SALAHUDDIN, F. KHAN (2017) Boundary layer flow of MHD tangent hyperbolic nanofluid over a stretching sheet: A numerical investigation. *Results in Physics* **7** 2837-2844.

[23] T. HAYAT, M. WAQAS, A. ALSAEDI, G. BASHIR, F. ALZAHRANI (2017) Magnetohydrodynamic (MHD) stretched flow of tangent hyperbolic nanoliquid with variable thickness. *Journal of Molecular Liquids* **229** 178-184.

[24] T. HAYAT, M. MUMTAZ, A. SHAFIQ (2017) Stratified magnetohydrodynamic flow of tangent hyperbolic nanofluid induced by inclined sheet. *Applied Mathematics and Mechanics* **38** 271-288.

[25] F. SHAHZAD, M. SAGHEER, S. HUSSAIN (2019) MHD tangent hyperbolic nanofluid with chemical reaction, viscous dissipation and Joule heating effects. *AIP Advances* **9** 1-11.

[26] K. MAQBOOL, S. SHAHEEN, A.M. SIDDIQUI (2019) Effect of Nano-Particles on MHD Flow of Tangent Hyperbolic Fluid in a Ciliated Tube: An Application to Fallopian Tube. *Mathematical Biosciences and Engineering* **16** 2927-2941.

[27] P.P. GHARAMI, S. REZA-E-RABBI, S.M. ARIFUZZAMAN (2020) MHD effect on unsteady flow of tangent hyperbolic nano-fluid past a moving cylinder with chemical reaction. *SN Applied Sciences* **2** 1-16.

[28] W.A. KHAN, I. POP (2010) Boundary-layer flow of a nanofluid past a stretching sheet. *International Journal of Heat and Mass Transfer* **53** 2477-2483.

[29] N.S. AKBAR, A. EBAI, Z.H. KHAN (2015) Numerical analysis of magnetic field effects on Eyring-Powel fluid flow towards a stretching sheet. *Journal of Magnetism and Magnetic Materials* **382** 355-358.

[30] M.Y. MALIK, T. SALAHUDDIN, A. HUSSAIN, S. BILAL (2015) MHD flow of tangent hyperbolic fluid over a stretching cylinder: Using Keller box method. *Journal of Magnetism and Magnetic Materials* **395**, 271-276.

[31] M. KHAN, A. HUSSAIN. M.Y. MALIK, T. SALAHUDDIN, F. KHAN (2017) Boundary layer flow of MHD tangent hyperbolic nanofluid over a stretching sheet: A numerical investigation. *Results in Physics* **7** 2837-2844.